Backscattering and common-base current gain of the Graphene Base Transistor (GBT)

Available online at www.sciencedirect.com

ScienceDirect

Microelectronic Engineering 00 (2015) 1–4

Journal Logo

Backscattering and common–base current gain of the Graphene Base Transistor (GBT)

Stefano Venica, Francesco Driussi, Pierpaolo Palestri, Luca Selmi

DIEG, University of Udine, via delle Scienze 208, Udine 33100, Italy

Abstract

In this paper, we investigate electron transport and electron scattering in the insulators of the Graphene Base Transistor (GBT) by means of a Monte Carlo transport model. We focus on electron backscattering in the base–collector insulator as the possible root cause of the large experimental base current and small measured common-base current gain (α_F) of GBTs. Different GBT structures have been simulated and the impact of the scattering parameters on the base current is analyzed. Simulated backscattering–limited α_F values are found to be much higher than available experimental data, suggesting that state-of-the-art technology is still far from being optimized. However, those simulated α_F values can be low enough to limit the maximum achievable GBT performance.

Keywords: Graphene Base Transistor, Monte Carlo method, Backscattering, Base current, Common–base current gain

1. Introduction

In the last decade, graphene has gained interest for its unique electrical properties, such as high electron mobility and high saturation velocity [1]. Unfortunately, the absence of a band–gap, makes graphene not suitable for digital circuit applications. In analog RF circuits instead, conventional MOSFET structures as the Graphene Field Effect Transistors (GFET) are able to reach a cut–off frequency (f_T) of about 400 GHz [2], but the non saturated behavior of output characteristics [3] causes the degradation of important RF figures of merit, as the intrinsic voltage gain $A_V = g_m/g_{ds}$. For this reason, new graphene based transistor concepts, as the Graphene Base Transistor (GBT, [4]), have been recently proposed that exploit quantum tunneling through thin dielectrics, as in the Hot Electron Transistor (HET, [5]). The GBT consists of a vertical structure (inset in Fig. 1), where a graphene sheet serves as the control electrode, the base (B), located at x=0 in Fig. 1. The base is separated from a metal or semiconducting emitter (E) and from a metal collector (C) by an emitter-base and a base-collector insulator (EBI and BCI, respectively) [4]. In normal operation (i.e. positive base–emitter bias, $V_{BE} > 0$ and positive collector–base bias, $V_{CB} > 0$), electrons tunnel through the EBI, cross the base perpendicularly to the graphene sheet (GR) and then drift across the conduction band (CB) of the BCI, following the x direction in Fig. 1. Despite its monoatomic thickness, the semi–metallic behavior of graphene ensures a very low base resistance, suggesting that the device can achieve high unity power gain frequencies (f_{MAX}) and high f_T values at the same time, overcoming the problems that strongly limit the HET performance [5]. In this respect, the DC functionality of GBT devices has been experimentally demonstrated [6, 7], and simulations predict cut-off frequencies in the THz range [8, 9, 10].

Ideally, the graphene base should be transparent to the flow of electrons, thus suggesting a null base current (I_B). In practice instead, experiments show a large I_B that severely limits the common-base current gain ($\alpha_F = I_C/I_E$, where I_C and I_E are the collector and emitter currents, respectively) [6, 7], meaning that graphene captures the majority of the travelling electrons. Two major capturing mechanisms are expected to be significant contributions to I_B: the first consists of the direct capture of the electrons impinging the EBI/graphene interface (direct capture), while the second is due to the electrons re–injected in the base by the backscattering events occurring in the conduction band of the BCI, and collected by the graphene.

In this framework, the aim of our contribution is to investigate the origin of the large measured base current and, in particular, to understand if I_B can be mainly attributed to the backscattering of electrons by the BCI. In the lack of a consolidated theoretical framework to compute the direct capture by the graphene, this contribution to I_B is neglected, making the calculated α_F an upper estimate of the actual one.

In the following, different GBT configurations have been simu-

Email address: venica.stefano@spes.uniud.it (Stefano Venica)

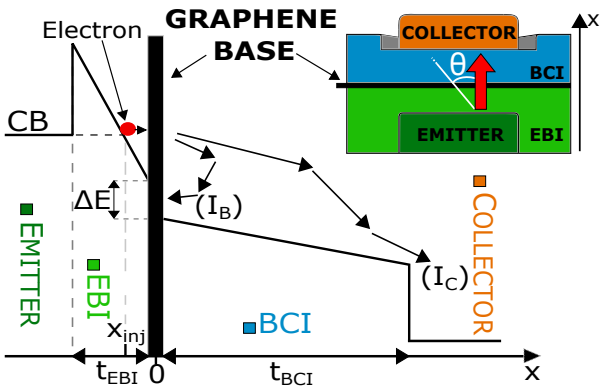

Figure 1. Conduction band diagram of the GBT. The electrons injected from the EBI through the graphene scatter in the BCI and either reach the collector (contributing to I_C) or backscatter to the base and are captured by the graphene (thus contributing to I_B). The inset shows the GBT structure and the definition of the backscattering angle θ.

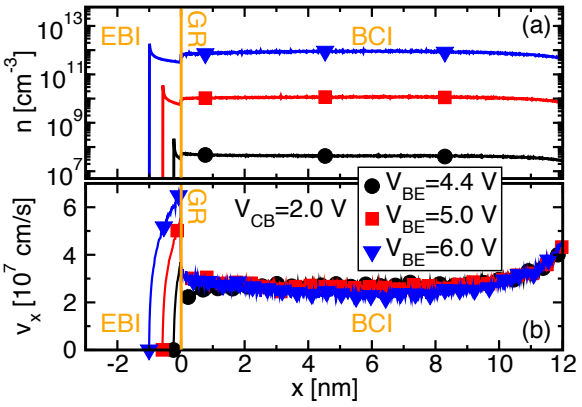

Figure 2. Average electron concentration (a) and average electron velocity (b) along a GBT device with EBI and BCI made of SiO_2 (t_{EBI}=3.0 nm, t_{BCI}=12 nm) for a few values of V_{BE}.

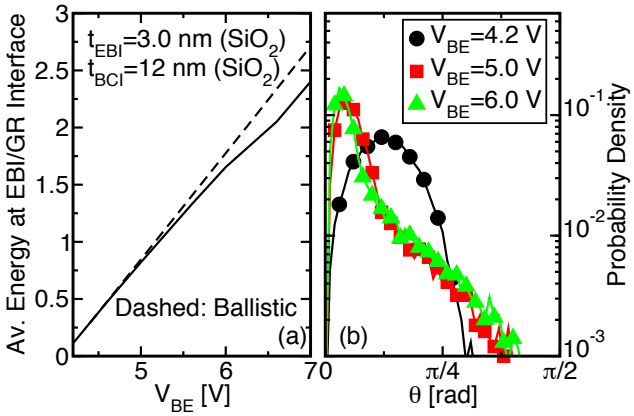

Figure 3. Electron energy (a) and probability distribution of the angle of incidence θ (inset in Fig. 1) (b) at the EBI/GR interface (x=0 in Fig. 1). Ballistic electron transport is reported as a reference in plot (a) (dashed line).

lated, to study which parameter impacts the backscattering and limits α_F.

2. Monte Carlo Transport Model

In order to evaluate the contribution of the backscattering to the degradation of α_F in GBT devices, we developed a dedicated Monte Carlo simulator for electron transport in the conduction band of the EBI and BCI. Consistently with [9], we neglect hole injection from the graphene to the EBI, since it is expected to provide a negligible reduction of the emitter efficiency and hence of α_F.

During the GBT operation, electrons are injected from the emitter toward the collector by tunneling; with a sufficiently high V_{BE}, Fowler–Nordheim tunneling through the EBI barrier takes place and electrons are injected in the conduction band of the EBI at x_{inj} (Fig. 1) with an energy that corresponds to the Fermi level in the emitter. For electrons crossing the graphene base, we assumed conservation of the electron momentum parallel to the graphene plane and of the total energy. After crossing the graphene, electrons reach the conduction band of the BCI. During the motion in the conduction band of the dielectrics, the electrons are subjected to many scattering events that can deflect their trajectory depending on the type of the collision occurred. In this respect, we include in the simulator both emission and absorption of polar optical and non–polar acoustic phonons, extending the model presented in [11] to a non–parabolic conduction band material, with a non–parabolicity coefficient α (see Tab. 1). We have verified the developed model by comparing the simulated electron average velocity in a SiO_2 slab to the results reported in [11].

The developed Monte Carlo tool is of the single–particle type, so it injects in the device one electron at a time. Electron free flights and scattering events are alternated until the particle exits the GBT, either arriving to the collector terminal from the BCI with positive velocity (thus contributing to I_C), or impinging the graphene layer with negative velocity due to backscattering in the BCI (thus contributing to I_B, Fig. 1). In this latter case, the scattering events occurring in the BCI (mostly in proximity of the graphene/BCI interface) deviate electron trajectory toward the graphene base ($\theta > \pi/2$). In particular, we consider an electron as captured by the base every time it impinges on the graphene; hence, we discard the possibility that such electron can be injected back again in the BCI conduction band. By knowing the amount of electrons that are exiting through the collector and the ones captured by the base during the simulation, we are able to estimate $\alpha_F = I_C/(I_C + I_B)$.

3. Simulation Results

Since calibrated scattering parameters are available for SiO_2, we start with simulations of GBTs with both EBI and BCI made of this material. The parameters are reported in Tab. 1 [12]. Then, in order to compare with the experiments in [6], we analyze GBTs with different high-k dielectrics, as those used for the EBI and BCI of optimized GBTs [8, 9, 10].

3.1. GBTs with SiO_2 EBI and BCI

Fig. 2 shows the electron concentration ($n(x)$) and the average velocity ($v_x(x)$) along the transport direction in a GBT

with t_{EBI}=3.0 nm and t_{BCI}=12 nm for a few V_{BE} values. As expected, the injection point x_{inj} moves backward as V_{BE} is increased due to the larger conduction band bending. The electron concentration is calculated according to the relation $n(x) = J_C/(q \cdot v_x(x))$, where J_C is the GBT collector current density simulated with the electrical model presented in [10] and $v_x(x)$ is given by the Monte Carlo simulation. In the EBI, $n(x)$ decreases along x (Fig. 2a), because electrons are accelerated (Fig. 2b) by the strong electric field. In the BCI, instead, the electron concentration and the average velocity along x are essentially constant. These simulations verify the important assumption made in the development of the model in [10], where we assumed a constant electron drift velocity ($v = 10^7$ cm/s) in the dielectrics when accounting for space charge effects.

Fig. 3a shows the average kinetic energy of electrons at the EBI/graphene interface computed with (solid line) and without scattering (dashed line). Since the thickness of the EBI (t_{EBI}) is quite limited, scattering induces only a small energy relaxation in the EBI layer. Fig. 3b reports the probability density of the angle θ (defined in the inset in Fig. 1) between the electron velocity and the x axis for the electrons hitting the EBI/graphene interface from the insulator side. By increasing V_{BE}, the distribution peak approaches θ=0, since the electric field strongly directs all the electrons toward the base.

Concerning the transport in the BCI, for increasing V_{BE}, the average kinetic energy of electrons entering the BCI is larger (Fig. 3a), hence, the average number of backscattering events in the BCI increases, consequently increasing I_B and reducing α_F (Fig. 4). In addition, by increasing the BCI thickness (t_{BCI}), the field in the BCI decreases, leading to more backscattering and further reducing α_F (Fig. 4b). This reduction, however, is modest as can be easily understood noting that in our model α_F is given by $(1 - r)$, where $r = I_B/I_E$ is the backscattering coefficient in the BCI. For large α_F values, r is small and large percentage variations of r result in small percentage variation of α_F (e.g. by changing t_{BCI} from 10 nm to 20 nm, r varies by 28% whereas α_F by 6% only; see Fig. 4b at high V_{BE}).

As for the t_{BCI} dependence, by increasing the EBI thickness (t_{EBI}) for given V_{BE} and V_{CB}, α_F reduces as shown in Fig. 4a, since the electrostatics of the device leads to a lower electric field in the BCI.

Optimized GBTs typically feature different materials for the EBI and BCI [8, 9, 10]. In this case, by denoting with χ_{EBI} and χ_{BCI} the affinity of the EBI and BCI, respectively, a conduction band discontinuity ΔE=(χ_{BCI}-χ_{EBI}) is present at x=0 (Fig. 1). In this respect, for ΔE>0, the average kinetic energy of electrons entering the BCI and the fraction of electrons that suffer backscattering increase, further reducing α_F (Fig. 4a, empty symbols). Hence, the use of dielectrics with very different affinities can be detrimental for α_F.

3.2. Comparison with experimental data

To compare the model with available data [6], we also simulated a GBT structure with 5.0 nm SiO_2 layer as EBI and 25 nm Al_2O_3 layer as BCI. Scattering parameters are those in Tab. 1, where the Al_2O_3 acoustic phonon scattering deformation potential C_{ae} is tentatively set equal to that of SiO_2. Simulated α_F are reported in Fig. 5. Similarly to Fig. 4, as V_{BE} increases, the kinetic energy of the electrons entering in the BCI conduction band increases, thus enhancing the probability of the electron to be backscattered in the graphene base. On the other hand, by increasing V_{CB}, the increase of the BCI electric field favors the electron drift toward the collector terminal, leading to higher α_F. Such V_{BE} and V_{CB} dependencies are consistent with the experiments of [6] (not shown). However, the calculated α_F values (0.5 ÷ 0.9) are much larger than the available measurements (10^{-3} ÷ 7×10^{-2}) [6, 7], but still small enough to pose a

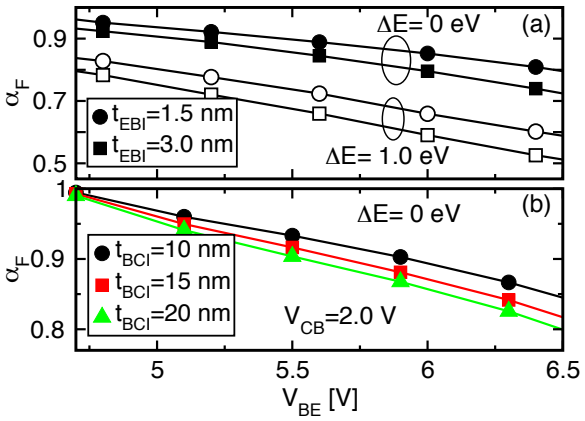

Figure 4. α_F versus V_{BE} for different EBI thickness (t_{EBI}) and ΔE for t_{BCI}=12 nm (a) and for different BCI thickness (t_{BCI}) with t_{EBI}=2.0 nm (b). In all the proposed configurations, SiO_2 parameters (Tab. 1) are used both for EBI and BCI, with the only exception of the open symbols in plot (a), which are obtained enforcing ΔE=1 eV by imposing a different affinity χ_{BCI}.

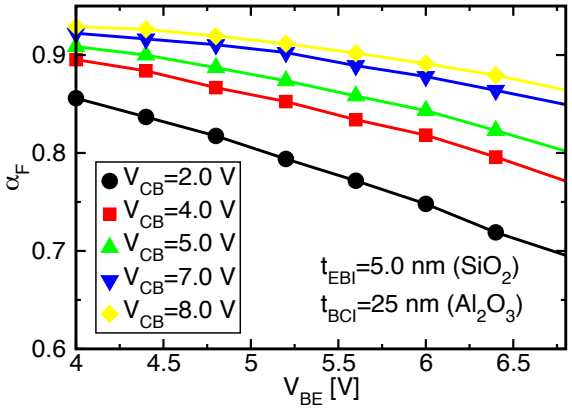

Figure 5. Simulated α_F as a function of V_{BE} for a GBT with EBI in SiO_2 and BCI in Al_2O_3. Scattering parameters as in Tab. 1.

Table 1. Scattering parameters used in the simulations of Figs. 2, 3, 4 and 5. SiO_2 parameters from [12].

	χ_I eV	m_I m_0	α eV^{-1}	ε_{stat} ε_0	ε_{int} ε_0	ε_∞ ε_0	ω_{LO1} meV	ω_{LO2} meV	C_{ae} eV
SiO_2	0.95	0.5	0.2	3.9	3.15	2.19	153	63	2.1
Al_2O_3	1.65 [13]	0.4 [13]	0.2	10 [13]	7.27 [14]	3.2 [14]	109 [15]	63.3 [15]	2.1

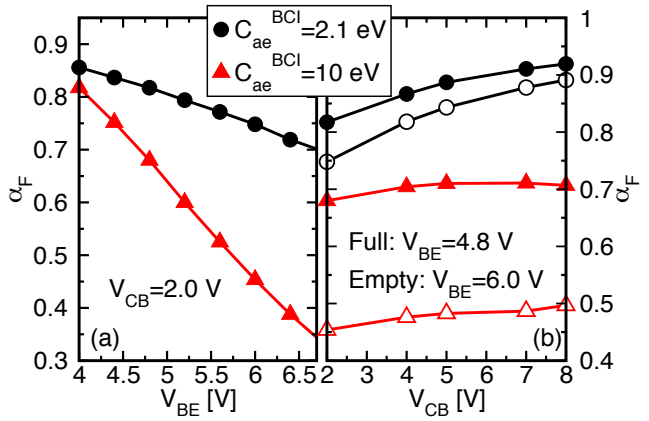

Figure 6. Simulated α_F as a function of V_{BE} (a) and V_{CB} (b) for the GBT of Fig. 5. C_{ae} of BCI is used as a free parameter.

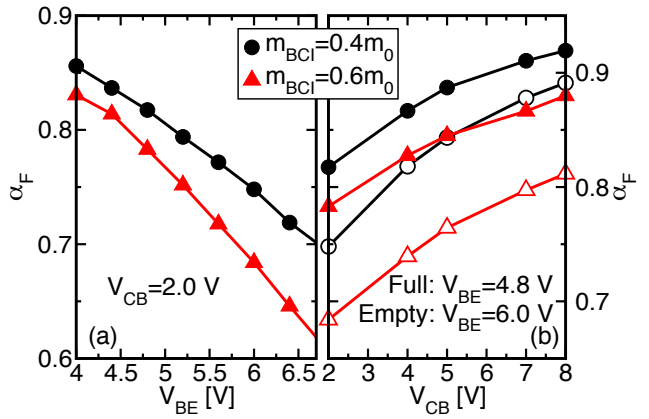

Figure 7. Simulated α_F as a function of V_{BE} (a) and V_{CB} (b) for the GBT of Fig. 5 and by using m_{BCI} as a free parameter.

severe limit to the GBT static performance.

If the scattering probability in the BCI is increased by choosing C_{ae} as high as 10 eV, we see a decrease of α_F (compare triangles vs. circles in Fig. 6a), but not enough to match the measurements. Moreover, the dependence of α_F on V_{CB} becomes weaker (Fig. 6b), since the larger probability of backscattering due to the increase of C_{ae} contrasts the effect of the higher electric field.

Finally, an increase of the conduction band mass in Al_2O_3 up to $0.6m_0$ (possibly justified by the large electron–phonon coupling in Al_2O_3 [16, 15]) lowers α_F, but again not enough to match the experiments, as illustrated in Fig. 7.

4. Conclusions

We developed a Monte Carlo transport simulator to investigate the effect of the scattering in the dielectrics on the operation of GBTs. The simulations point out that the average electron velocity along the BCI is rather constant and in the order of 10^7 cm/s, thus verifying the assumptions previously made in [10], when including the space charge effects in the GBT electrical model.

As regards α_F, even accounting for the unavailable uncertainties on the scattering parameters, it is not possible to reconcile simulations with experiments. This may also indicate that additional physical mechanisms (e.g. interface traps and direct electron capture by the graphene) are responsible for the low measured α_F. Nevertheless, our results underline that electron backscattering from the BCI to the graphene base can pose a severe limit to α_F.

5. Acknowledgments

This research activity has received funding by the UE through the STREP project GRADE (317839). The authors acknowledge D. Esseni (University of Udine), S. Vaziri (KTH) and M. C. Lemme (University of Siegen) for fruitful discussions.

References

[1] V. E. Dorgan, M.-H. Bae, E. Pop, "Mobility and saturation velocity in graphene on SiO2", *Applied Physics Letters* 97 (8) (2010) 082112.
[2] R. Cheng, J. Bai, L. Liao, H. Zhou, Y. Chen, L. Liu, Y.-C. Lin, S. Jiang, Y. Huang, X. Duan, "High-Frequency Self–Aligned Graphene Transistors with Transferred Gate Stacks", *Proceedings of the National Academy of Sciences* 109 (29) (2012) 11588–11592.
[3] S. Rodriguez, S. Vaziri, M. Ostling, A. Rusu, E. Alarcon, M. C. Lemme, "RF Performance Projections of Graphene FETs vs. Silicon MOSFETs", *ECS Solid State Letters* 1 (5) (2012) Q39–Q41.
[4] W. Mehr, J. Dabrowski, J. Christoph Scheytt, G. Lippert, Y.-H. Xie, M. C. Lemme, M. Ostling, G. Lupina, "Vertical Graphene Base Transistor", *IEEE Electron Device Letters* 33 (5) (2012) 691–693.
[5] M. Heiblum, M. Fischetti, "Ballistic Hot–Electron Transistors", *IBM Journal of Research and Development* 34 (4) (1990) 530–549.
[6] S. Vaziri, G. Lupina, C. Henkel, A. D. Smith, M. Östling, J. Dabrowski, G. Lippert, W. Mehr, M. C. Lemme, "A Graphene-Based Hot Electron Transistor", *Nano Letters* 13 (4) (2013) 1435–1439.
[7] C. Zeng, E. B. Song, M. Wang, S. Lee, C. M. Torres, J. Tang, B. H. Weiller, K. L. Wang, "Vertical Graphene-Base Hot-Electron Transistor", *Nano Letters* 13 (6) (2013) 2370–2375.
[8] F. Driussi, P. Palestri, L. Selmi, Modeling, simulation and design of the vertical Graphene Base Transistor , *Microelectronic Engineering* 109 (2013) 338–341.
[9] V. Di Lecce, R. Grassi, A. Gnudi, E. Gnani, S. Reggiani, G. Baccarani, "Graphene Base Transistors: A Simulation Study of DC and Small-Signal Operation", *IEEE Transactions on Electron Devices* 60 (10) (2013) 3584–3591.
[10] S. Venica, F. Driussi, P. Palestri, D. Esseni, S. Vaziri, L. Selmi, "Simulation of DC and RF Performance of the Graphene Base Transistor", *IEEE Transactions on Electron Devices* 61 (7) (2014) 2570–2576.
[11] M. V. Fischetti, D. J. DiMaria, S. D. Brorson, T. N. Theis, J. R. Kirtley, "Theory of High-Field Electron Transport in Silicon Dioxide", *Physical Review B* 31 (1985) 8124–8142.
[12] P. Palestri, L. Selmi, M. Pavesi, F. Widdershoven, E. Sangiorgi, "Coupled Monte Carlo Simulation of Si and SiO_2 Transport in MOS Capacitors", *Proceedings of SISPAD* (2000) 38–41.
[13] S. Spiga, F. Driussi, A. Lamperti, G. Congedo, O. Salicio, "Effects of Thermal Treatments on the Trapping Properties of HfO 2 Films for Charge Trap Memories", *Applied Physics Express* 5 (2) (2012) 021102.
[14] M. V. Fischetti, D. A. Neumayer, E. A. Cartier, "Effective electron mobility in Si inversion layers in metaloxidesemiconductor systems with a high- insulator: The role of remote phonon scattering", *Journal of Applied Physics* 90 (9) (2001) 4587–4608.
[15] J. Shan, F. Wang, E. Knoesel, M. Bonn, T. F. Heinz, "Measurement of the Frequency-Dependent Conductivity in Sapphire", *Physical Review Letters* 90 (2003) 247401.
[16] V. G. Kravets, "Polaron interpretation of the magnetoreflectance effect in insulating αAl_2O_3", *Physical Review B* 72 (2005) 064303.